Atmospheric Research 248 (2021) 105217

Contents lists available at ScienceDirect

Atmospheric Research

journal homepage: www.elsevier.com/locate/atmosres

Investigation of the relationship between the fine mode fraction and Ångström exponent: Cases in Korea

Ja-Ho Koo[a], Juhee Lee[b], Jhoon Kim[a], Thomas F. Eck[c], David M. Giles[c], Brent N. Holben[c], Sang Seo Park[d], Myungje Choi[a], Najin Kim[a], Jongmin Yoon[e], Yun Gon Lee[b,*]

[a] Department of Atmospheric Sciences, Yonsei University, Seoul, Republic of Korea
[b] Department of Atmospheric Sciences, Chungnam National University, Daejeon, Republic of Korea
[c] NASA Goddard Space Flight Center, Greenbelt, MD, USA
[d] School of Urban and Environmental Engineering, Ulsan National Institute of Science and Technology, Ulsan, Republic of Korea
[e] Climate and Air Quality Research Department, National Institute of Environmental Research, Incheon, Republic of Korea

ARTICLE INFO

Keywords:
Ångström exponent
Fine mode fraction
Hygroscopic growth
AERONET

ABSTRACT

Based on long-term AERONET observations in the Korean peninsula, we evaluate how well the Ångström exponent (AE) can describe the regional aerosol size well in comparison to the fine mode fraction (FMF). Despite close relationships between AE and FMF previously reported, we found that AE is not always linearly correlated to the FMF in the Korean peninsula, particularly during the summertime. Seasonal patterns of volume size distribution indicate that the volume median and peak radius of the fine mode are obviously enhanced in the summer. Since the ambient conditions in Korean summer are highly humid, cloudy, and stagnant, the size of regional fine mode aerosol can increase significantly due to hygroscopic growth and/or cloud processing in this highly polluted atmosphere. In contrast to the AE, the AE ratio (AE at longer wavelengths divided by AE at shorter wavelengths; AER) correlates better with the FMF variation in summer, but a little worse in the spring. This suggests that the combined consideration of AE and AER may provide a better characterization relative to FMF. Thus, we try to estimate the FMF based on the multiple linear regression method using both AE and AER. As expected, the estimated FMF shows remarkably high linear correlations with the AERONET FMF without any seasonal bias. These findings imply that the FMF in South Korea can be simply obtained if just the AOT measurement at multiple wavelengths (in the range from ultraviolet to near-infrared channels) are available.

1. Introduction

Aerosol optical properties have been intensively investigated over the last few decades to more fully figure out the role of airborne aerosols in various processes. These properties are critical to characterize the extent of aerosol radiative forcing: the amount of absorption or scattering of solar radiation due to the regional aerosols. Since each aerosol type has distinctive characteristics, aerosol type classification is necessary task in order to compute exact radiative forcing calculations (e.g., Lee et al., 2014; Alam et al., 2018; Yoon et al., 2019). Aerosol size is one of the essential parameters required for the determination of most aerosol types (e.g., Lee et al., 2010; Verma et al., 2015), generally composed of fine (sub-micron radius) and coarse modes (super-micron radius). In particular, the aerosol size distribution significantly affects the aerosol scattering efficiency (Valentini et al., 2020), which is a major component in the estimation of radiative forcing. Thus, the determination of qualifiable aerosol size information is necessary.

Aerosol size distribution information for the entire atmospheric column has been retrieved using the ground-based remote sensing measurements of spectral aerosol optical thickness (AOT) and directional sky radiances. The Aerosol Robotic Network (AERONET) is the well-known international platform to perform this monitoring. Using the pattern of spectral AOT, the bimodal aerosol size distribution, fine and coarse mode, can be derived (O'Neil and Royer, 1993). The ratio of these two modes, fine mode fraction (FMF) is the representative information about the local aerosol size, describing the portion of fine mode aerosols in the local atmosphere that contribute to the total AOT. The AERONET has provided FMF using the spectral deconvolution algorithm (SDA) based on the measurement of direct solar radiance (O'Neill et al., 2001; O'Neill et al., 2003). Inversions of measurements made by the AERONET have also estimated columnar FMF of AOT

* Corresponding author.
E-mail address: yglee2@cnu.ac.kr (Y.G. Lee).

https://doi.org/10.1016/j.atmosres.2020.105217
Received 3 March 2020; Received in revised form 6 July 2020; Accepted 4 August 2020
Available online 29 August 2020

(Dubovik et al., 2002, 2006). These inversions are very useful, however, they require a relatively cloudless sky radiance scan (almucantar) made at solar zenith angle > 50 degrees as input to the inversion process of AERONET algorithm. These two FMFs are basically consistent but sometimes show some differences (Eck et al., 2010; Zheng et al., 2019).

The Ångström exponent (AE) is also well-known parameter estimated from the spectral measurement of AOT. The basic assumption for AE was that it is assumed to be almost constant with wavelength as the linear regression of AOT versus wavelength in logarithmic scale. This AE has been widely utilized to characterize some general information on relative aerosol size (Eck et al., 1999). Many previous studies have indicated that the small magnitude of AE implies the coarse-mode particle dominance, and vice versa (e.g., Dubovik et al., 2002; Kim et al., 2004; Xin et al., 2007). In some regions, AE is highly correlated with FMF (Eck et al., 2008), suggesting that AE may be a good proxy as an indicator of the relative influence of the two primary size modes. Thus, AE has been also used in some methods of aerosol type classification in order to account for some differences in particle size (Lee et al., 2018; Logothetis et al., 2020).

Recently, a number of studies showed that the AE varies significantly as a function of wavelength (Eck et al., 1999; Kaskaoutis and Kambezidis, 2006; Soni et al., 2011), and the sensitivity of AE to the aerosol size information is highly dependent on the selected wavelength range of the AOT utilized in the computation (Schuster et al., 2006). While the AE at 440 and 870 nm has been widely used as a general particle size indicator for fine versus coarse mode relative influence, it is also important to consider the wavelength dependence of AE for better quantification of aerosol size (Eck et al., 1999; Gobbi et al., 2007; Yoon et al., 2012). Moreover, recent studies revealed that the AE at 440–870 nm sometimes cannot describe the relative aerosol size well. Some previous works already revealed that the reduction of AE can happen associated with the growth of fine mode aerosols, which is the reason why there is sometimes a negative correlation between AOT and AE (Reid et al., 1999; O'Neill et al., 2001, 2003). Eck et al. (2012) reported this issue in analysis of AERONET data in polluted regions showing high relative humidity (RH). They explained this irregular pattern of AE (small AE yet still fine mode dominated) as a result of aging and/or hygroscopic growth (fog- and cloud-processing) of particles under humid and stagnant air conditions.

The Korean peninsula located in East Asia is often subject to severe air pollution in close proximity to a marine basin, Yellow Sea (Lee et al., 2019), therefore may have some issues in AE usage when high RH or clouds are present. Thus, the focus of this study is the diagnosis of the utilization of AE to characterize FMF using the ground-based AERONET measurements of spectral AOT only at multiple sites in the Korean peninsula. We also analyze the spectral pattern of AE in terms of the regional conditions. Finally, we develop another way to better estimate FMF from spectral AE using a statistical approach.

2. Data description

This study mainly investigates parameters based on aerosol optical properties measured and retrieved from the AERONET observation (Holben et al., 1998) sites in the Korean peninsula (Level 2.0 dataset). Among all Korean AERONET sites, we select six sites that have conducted monitoring for a minimum 2 years, a suitable period for investigating general patterns: Anmyon, Baengnyeong, Gangneung-Wonju national university (hereafter Gangneung_WNU), the Gosan site on Jeju island established by the Seoul National University (hereafter, Gosan_SNU), Gwangju Institute of Science and Technology at Gwangju (hereafter Gwangju_GIST), and Yonsei University in central Seoul (hereafter Yonsei_Univ) (Fig. 1 and Table S1). Considering the site locations in Fig. 1, data from these six sites can represent latitudinal (South to North) and longitudinal (West to East) gradients or patterns on the southern Korean peninsula.

Multiple aerosol optical properties can be obtained from the

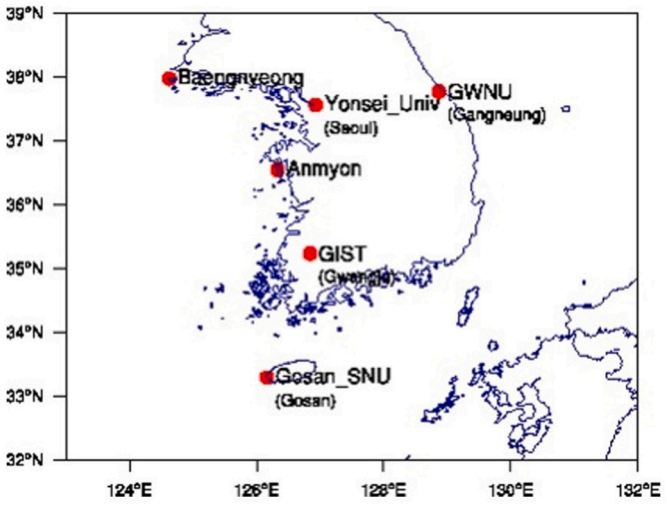

Fig. 1. Six Korean AERONET stations used in this study. All stations have measurements longer than 2 years.

AERONET data archive (https://aeronet.gsfc.nasa.gov). Spectral AOT (340 to 1640 nm in 8 narrow band-pass channels) is the basic parameter among aerosol optical properties, revealing the atmospheric turbidity or total column integrated light extinction by airborne particles (Mok et al., 2018). AE can be estimated based on the spectral dependence of AOT, defined as the slope value of the linear regression between AOTs and their respective wavelengths in a logarithmic scale. The AE estimated in the range between 440 and 870 nm (hereafter, $AE_{440\text{-}870nm}$) is provided in the AERONET database (computed from 4 channels: 440, 500, 675, and 870 nm) and is generally considered as associated with the investigation of relative modal contribution to AOD (e.g., Schuster et al., 2006). In addition to $AE_{440\text{-}870nm}$, AE values from other wavelengths are also computed in the AERONET database as a regression of three wavelengths. The AERONET data archive also provides the FMF, officially at 500 nm (hereafter, FMF_{500nm}) using both SDA (O'Neill et al., 2001; O'Neill et al., 2003) and inversion (Dubovik et al., 2002, 2006) algorithms. To examine the seasonal change of regional aerosol size pattern, we also analyze the volume size distribution retrieved from almucantar sky scans by the AERONET inversion algorithm (Dubovik and King, 2000; Dubovik et al., 2006). Recently, these aerosol optical properties were updated based on new AERONET data products: version 3 (Eck et al., 2018; Giles et al., 2019). All results in this study are produced using the version 3 data, but analyses based on the version 2 data (Holben et al., 2006) are also compared for the validation purposes, attached in the Appendix.

To investigate the meteorological effect to the aerosol properties, we also utilized several meteorology data (e.g., cloud fraction, relative humidity, and wind speed) provided from observations of the automatic weather station (AWS) managed by the Korean Meteorological Administration (KMA). To examine the influence of local air chemical pattern, we also used the aerosol component information (black carbon, organic carbon, mineral dust, and sea salt) of the Modern-Era Retrospective analysis for Research and Applications version 2 (MERRA-2) reanalysis dataset (Randles et al., 2007), and the surface measurement of air pollutants obtained from the AIRKOREA network (https://www.airkorea.or.kr): particulate matter having a diameter smaller than 10 μm (PM_{10}), nitrogen dioxide (NO_2), Sulfur dioxide (SO_2), ozone (O_3), and carbon monoxide (CO). Comparison between extremely high and low level of each factor becomes useful to find a condition that we cannot use AE as a particle size indicator.

3. Results and discussions

3.1. Relationship between AE and FMF

A number of previous studies found a generally positive correlation between $AE_{440\text{-}870nm}$ and FMF_{500nm} (e.g., Anderson et al., 2005; Eck et al., 2008). Therefore, the $AE_{440\text{-}870nm}$ has been sometimes utilized as a proxy for information on the FMF. However, the positive correlation between AE and FMF does not always hold, particularly in polluted regions with significant moisture, and this somewhat anomalous feature was explained by the influence of fog- and cloud-processed fine-mode particle growth (Eck et al., 2012). Since the East Asian atmosphere is heavily polluted, and often subjected to very humid conditions (Kim et al., 2007), this issue for the relationship between AE and FMF can be similarly seen in the Korean peninsula. Thus, we would compare between $AE_{440\text{-}870nm}$ and FMF_{500nm} at the six selected sites in Korea to see what really happens. We use the FMF provided from both the SDA and inversion algorithms, but we put the discussion related to the FMF from the SDA algorithm first because the larger number of SDA algorithm data can be resulted in more reliable analyses. Then we add some comparisons to the result about the FMF from the inversion algorithm.

At first, we performed a linear correlation analysis between $AE_{440\text{-}870nm}$ and FMF_{500nm} at the six selected sites in Korea. Results (Fig. 2) show that the positive correlation between $AE_{440\text{-}870nm}$ and FMF_{500nm} from the SDA algorithm is generally high. The correlation coefficient (R) is higher than 0.85 for all sites in spring (March–April-May, MAM), and R is ~0.6 to 0.8 in autumn (September–October-November, SON) and winter (December–January-February, DJF). In summer, however, the correlation becomes relatively weak at some sites (as low as $< \sim 0.1$). The positive relationship is maintained when both FMF_{500nm} and $AE_{440\text{-}870nm}$ are small. But the correlation collapses when the FMF_{500nm} is relatively high due to the wide range of $AE_{440\text{-}870nm}$. As a result, $AE_{440\text{-}870nm} > 1.0$ loses the sensitivity in some seasons to determine the dominance of regional modal aerosol size. Except for the Gosan_SNU site located in Jeju island (~100 km from the south coast of the Korean peninsula), other five sites consistently indicate relatively very low AE-FMF correlations in summer. Considering previous findings (e.g., Eck et al., 2012, 2014), this feature means that summertime particle size distributions in most of South Korea contain enough mid-sized submicron particle to cause a degradation of the effectiveness of $AE_{440\text{-}870nm}$ capability as a particle size indicator. Here, we would also underline that the degradation of AE-FMF relationship is stronger and occurs extensively over the whole Korean peninsula, compared to reported cases before (Eck et al., 2010, 2012).

We examine the monthly variation of several meteorological factors to better figure out the irregular AE-FMF relationship in the Korean summer. Based on the monthly mean patterns of RH, cloud fraction, and wind speed at six target sites (Fig. 3), summertime ambient conditions in the Korean peninsula are very humid and stagnant; RH and cloud fraction is the highest and the wind speed is the lowest in summer. In this environment, aerosol size can increase through the hygroscopic growth and coagulation process plus fog- and cloud-processing of particles (Eck et al., 2012). Actually, it has been known that the monthly mean AOT in the Korean peninsula typically shows the highest peak in June (the summertime before the rainy season) attributed to these processes (Kim et al., 2007; Koo et al., 2016). Comparing the seasonal mean almucantar retrievals of volume size distribution of ambient aerosols at six target sites (Fig. 4), we can find that the peak radius of fine mode aerosol volume increases in summer at all six sites. This feature is consistent with the recent finding in Eck et al. (2020), showing the 10 times larger increase of particle volume on high RH days in the Korean peninsula. Here we can clearly confirm the summertime fine-mode aerosol growth in the Korean peninsula.

These characteristics are similar to findings in Eck et al. (2012), suggesting that the existence of "large fine mode-dominated aerosols" can relate to the poor correlation between $AE_{440\text{-}870nm}$ and FMF_{500nm}. Two atmospheric situations are conducive to the growth of fine mode particles (resulted in the large dominance of fine mode aerosols locally): (1) high concentrations of fine mode aerosols and (2) ambient conditions with very high RH and the associated presence of clouds and

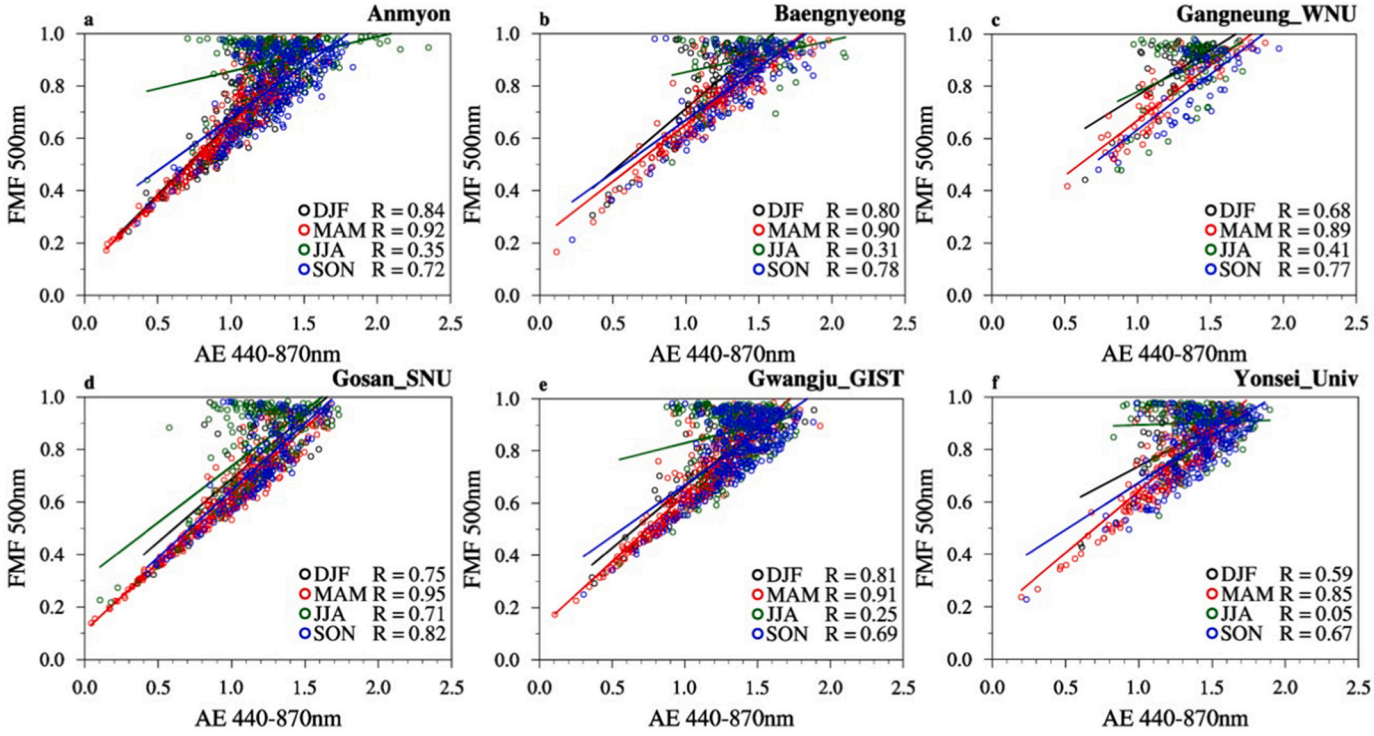

Fig. 2. Scatter plots showing the relationship between $AE_{440\text{-}870nm}$ and FMF_{500nm} from the SDA algorithm (version 3) for six sites: (a) Anmyon, (b) Baengnyeong, (c) Gangneung_WNU, (d) Gosan_SNU, (e) Gwangju_GIST, and (f) Yonsei_Univ. Correlation coefficients (R) were calculated for each season: December–January-February (DJF, black), March–April-May (MAM, red), June–July-August (JJA, green), and September–October-November (SON, blue).

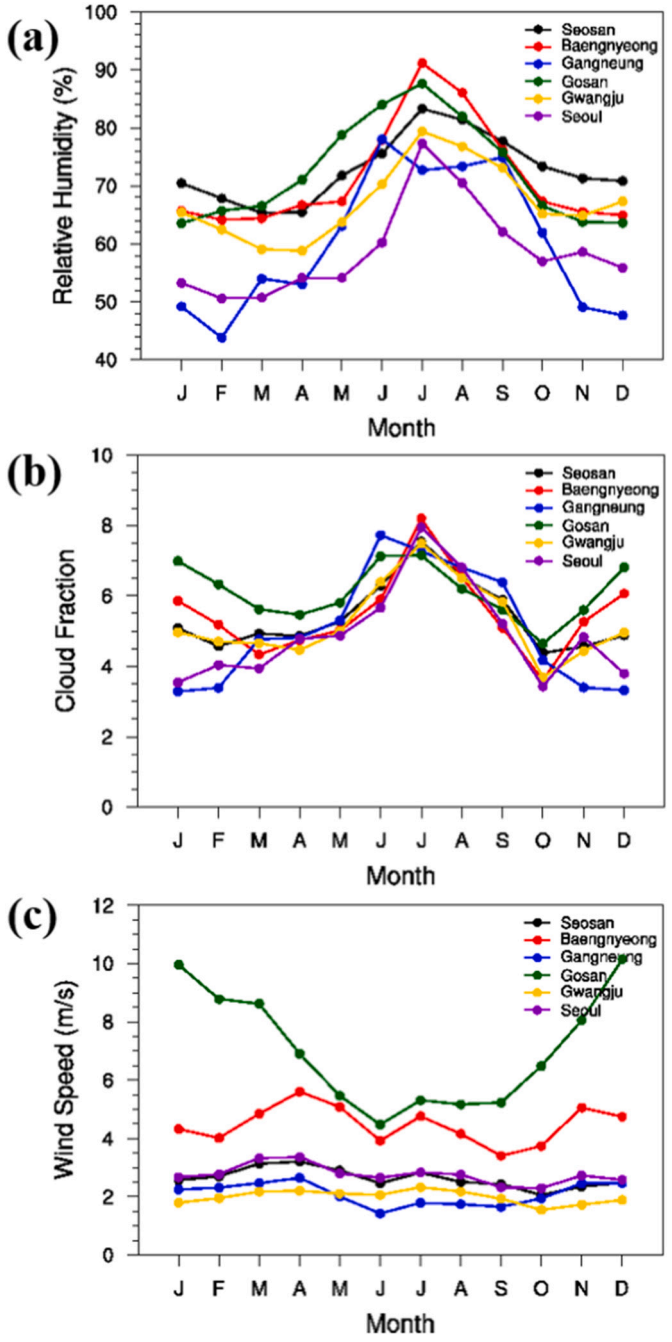

Fig. 3. Monthly mean pattern of (a) relative humidity, (b) cloud fraction, and (c) wind speed at six Korean AERONET sites. Seosan is the closest AWS of the AERONET Anmyon site, Baengnyeong is the closest AWS for the AERONET Bangnyeong site, Gangneung is the closest AWS for the AERONET Gangneung_WNU, Gosan is the closest AWS of the AERONET Gosan_SNU site, Gwangju is the closest AWS for the AERONET Gwangju_GIST site, and Seoul is the closest AWS for the AERONET Yonsei_Univ site.

fog. The Korean summer season, which is typically quite polluted in conjunction with a humid and stagnant atmosphere (Kim et al., 2007; Eck et al., 2020), satisfies these conditions in general. Some previous studies in East Asia also revealed that the hygroscopic growth of aerosol is more efficient for polluted condition than those for clear conditions (Kim et al., 2006; Yan et al., 2009). Relatively, the peak radius change of fine mode particle does not much increase at Gangneung_WNU and Gosan_SNU (Fig. 4) in spite of high RH. In this regard, the summertime correlation between AE and FMF at Gangneung_WNU and Gosan_SNU is not much degraded compared to other sites (Fig. 2). In contrast, the Yonsei_Univ site shows the increasing peak radius of fine mode aerosols in summer, clearly associated with the large degradation of the AE-FMF correlation. Considering that the Gangneung_WNU and Gosan_SNU site is located in relatively clean coastal area but the Yonsei_Univ site is located in the polluted megacity (Seoul), the extent of aerosol pollution looks significantly associated with the poor correlation between AE and FMF.

To investigate which ambient air conditions the most influential, we analyze the AE-FMF correlation deeply using the various information for local air chemicals and meteorology. For this analysis, we use the level of five surface air pollutants (PM_{10}, NO_2, SO_2, O_3, and CO), four aerosol components (black carbon, organic carbon, mineral dust, and sea salt), and three meteorological factors (wind speed, RH, and cloud fraction). Based on these data, we split the AE-FMF relationship into three groups according to the amount of considering variables: lower, middle, and higher percentiles of each variable. This approach reveals that which condition is strongly associated with the poor correlation between AE and FMF.

At first, we examine the AE-FMF correlation in terms of the level of surface air pollutants (Figs. S1, S2, S3, S4, and S5), but no obvious feature is discovered. Either extremely high or low level of air pollutants is not connected to the poor relation between AE and FMF, implying that only high air pollution itself is not the main condition to induce the poor AE-FMF correlation. When we consider the aerosol composition instead (Figs. S6, S7, S8, and S9), obvious patterns are not discriminated. While it seems that the dominance of fine mode aerosols (i.e., high percentiles of black carbon and organic carbon mass density) is a little more associated with the poor correlation between AE and FMF, different from the dominance of coarse mode aerosols (i.e., high percentiles of mineral dust and sea salt mass density), their difference is not meaningful. Thus, the level of ambient air pollution or the dominance of a certain aerosol type does not look influential to the occurrence of poor correlation between AE and FMF.

However, the result becomes much notable when we consider the meteorological factors, such as wind speed, RH, and cloud fraction (Figs. S10, S11, and S12); There is a separation in the AE-FMF relationship. In the Fig. 5, the obvious example at the Gwangju_GIST site, the linear correlation between AE and FMF is well found if the wind speed is high, RH is low, and cloud fraction is low. Reversely, the poor correlation between AE and FMF much happens with the low wind speed, high RH, and high cloud fraction. Here we do not consider the variation of air pollution level or aerosol composition, in other words, this separation is only driven by the consideration of local meteorology. Thus, this finding clearly indicates that the local meteorology is most important factor for explaining the poor quality of AE as a particle size indicator. In brief, when the local atmosphere is quite stagnant (i.e., low wind speed) and humid (high RH and cloud fraction), AE loses its capability to describe the size of local aerosols.

This feature basically supports well our analysis related to Figs. 3 and 4, addressing that the hygroscopic growth of aerosols under the humid and stagnant Korean summertime relates to the poor AE-FMF correlation. Moreover, here we noticed that the meteorological pattern should be more weighted rather than the air pollution level or aerosol types for the understanding of characteristics of AE and FMF. In the work of Eck et al. (2010), AE-FMF relationships were compared at three sites: Kanpur, India, Ilorin, Nigeria, and Beijing, China. All these sites have a serious air pollution, but the degradation of AE-FMF correlation is the strongest at the Beijing site, but the weakest at the Ilorin site. Eck et al. (2010) interpreted that this difference happens because the aerosol hygroscopicity differs according to its type (e.g., weak hygroscopicity for fresh biomass burning particles but the strong for aerosols from the fossil fuel combustions). The result in our study, however, implies that the ambient condition probably better explains the degradation of AE-FMF linear relationship. Namely, larger scatter of FMF at higher AE at Beijing reported in Eck et al. (2010) seems more related

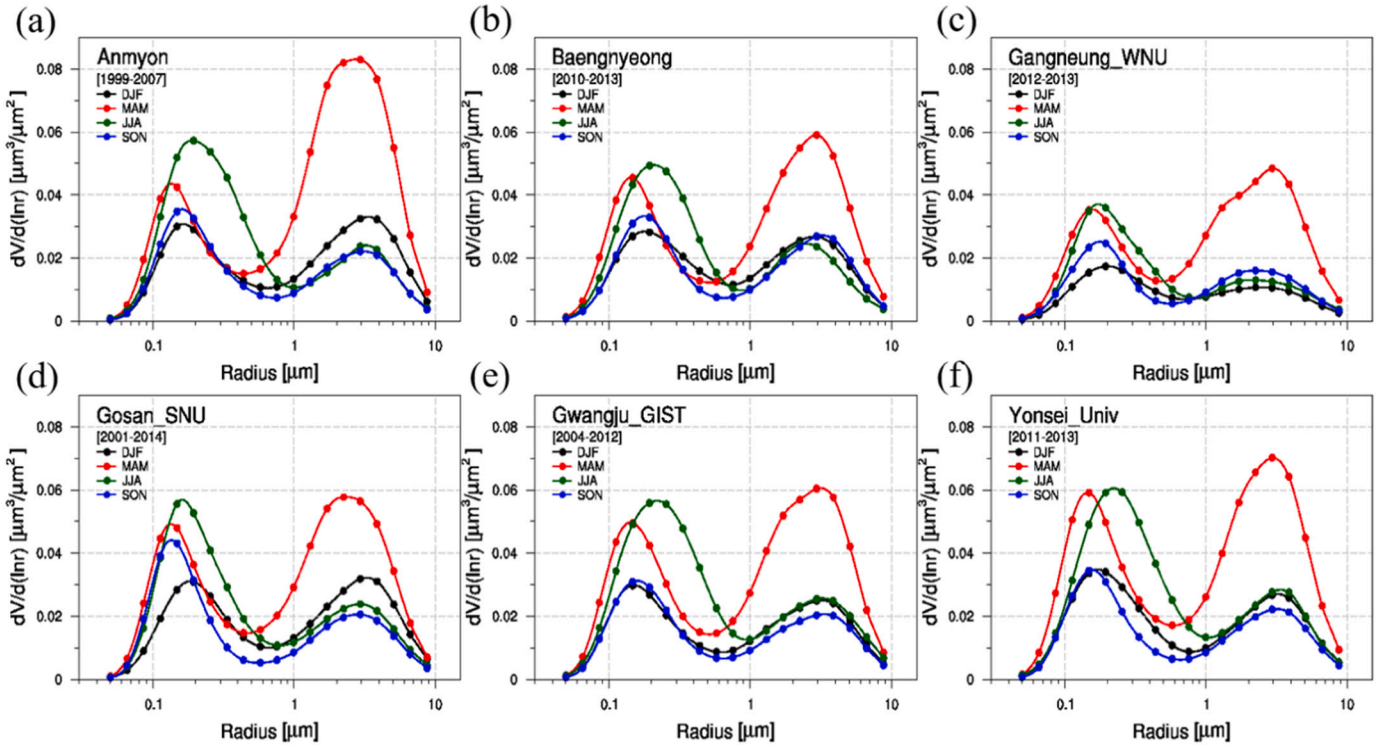

Fig. 4. Seasonal mean pattern of volume size distribution at six sites: (a) Anmyon, (b) Baengnyeong, (c) Gangneung_WNU, (d) Gosan_SNU, (e) Gwangju_GIST, and (f) Yonsei_Univ. Four seasons were compared: DJF (black), MAM (red), JJA (green), and SON (blue).

to the humid and stagnant condition in East Asian summer than the locally dominant aerosol type. We suggest that more seasonal analysis of aerosol optical properties will be required because the regional meteorology usually has a large seasonal variation.

3.2. Improvement of AE usage

Our results reveal that the degradation of the AE-FMF correlations can occur widely over the Korean peninsula during the entire summer, not limited to just some special events. Therefore, usage of the $AE_{440\text{-}870nm}$ as a proxy of aerosol size in this kind of environment is severely compromised. As mentioned above, the AERONET network provides FMF data based on their own algorithms, SDA algorithm (O'Neill et al., 2001; O'Neill et al., 2003) and almucantar sky scan inversion algorithm (Dubovik et al., 1998; Eck et al., 2012). But other remote sensing missions (e.g., satellites, shadowband instruments, etc.) still have difficulties to develop the algorithm producing accurate FMF values. AE values, however, can be easily obtained by AOT measurements from multiple channels, if high accuracy of AOT observation is guaranteed. Thus, it is still beneficial to find an improved way to use AE value directly as a particle size indicator.

Some previous studies have shown that the aerosol types can be classified using AE values from the different wavelength pairs (Gobbi et al., 2007; Koo et al., 2016), because the AE reflects the aerosol optical properties dissimilarly according to the wavelength used. For example, the curvature pattern of spectral AOD is opposite between the fine and coarse mode dominance (Eck et al., 1999). Even for the same aerosol type, the AE value is not perfectly same according to the selected wavelengths (Reid et al., 1999). In addition, it is known that the AE from long wavelengths has larger sensitivity to the fine mode volume fraction of aerosols, but AE from short wavelengths has larger sensitivity to the fine mode effective radius (Schuster et al., 2006).

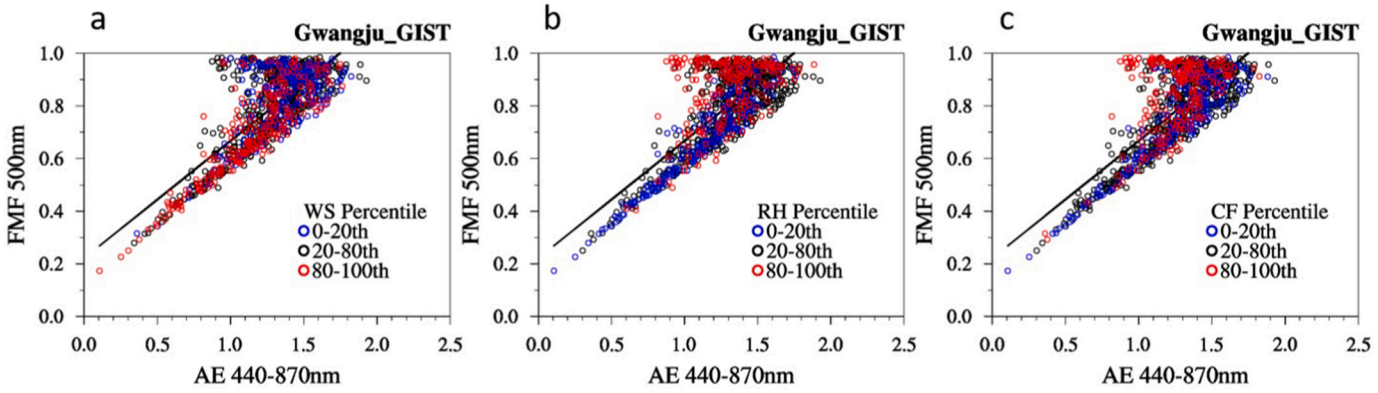

Fig. 5. Scatter plots showing the relationship between $AE_{440\text{-}870nm}$ and FMF_{500nm} from the SDA algorithm (version 3) at Gwangju_GIST sites. Here we simultaneously consider the extent of surface observed (a) wind speed, (b) relative humidity, and (c) cloud fraction: lower percentile (0-20th, blue dots), middle percentiles (20-80th, black dots), and higher percentiles (80-100th, red dots) of each variable.

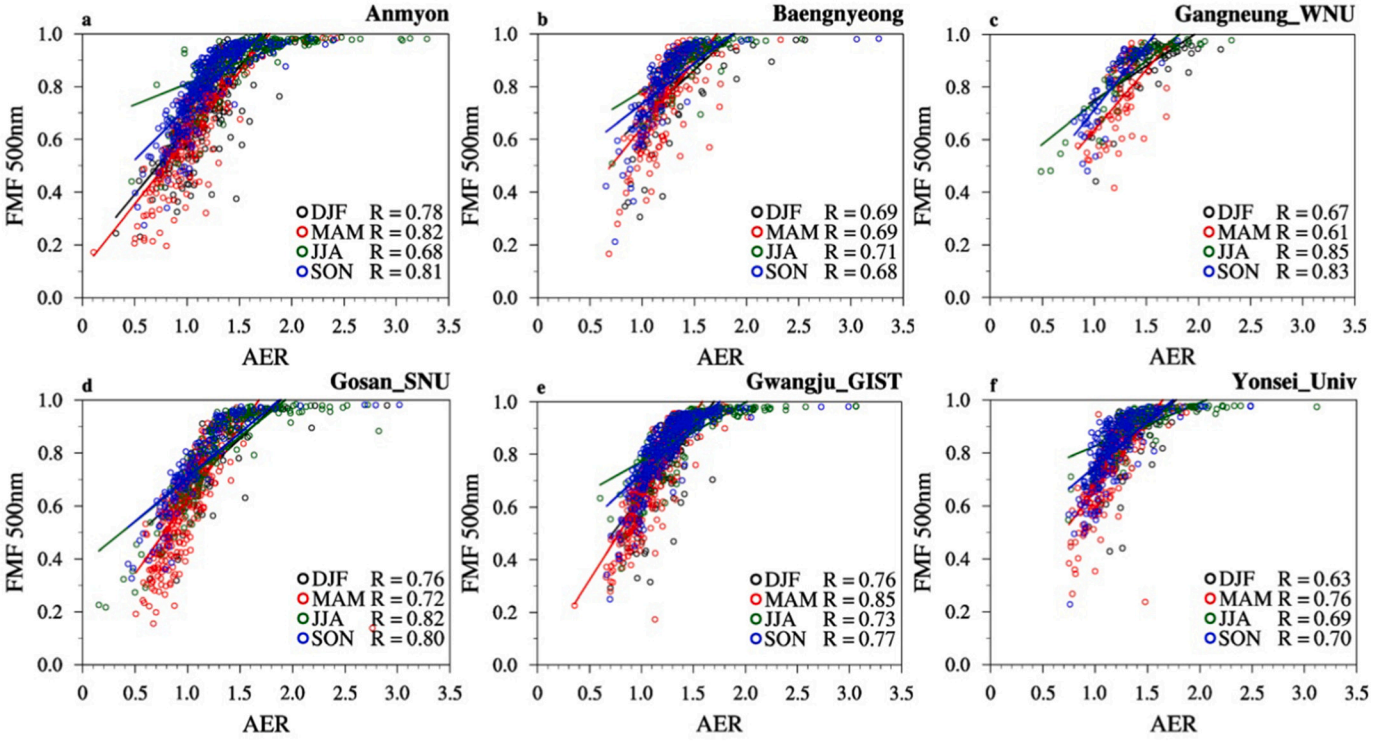

Fig. 6. Scatter plots showing the relationship between AER and FMF_{500nm} from the SDA algorithm (version 3) for six sites: (a) Anmyon, (b) Baengnyeong, (c) Gangneung_WNU, (d) Gosan_SNU, (e) Gwangju_GIST, and (f) Yonsei_Univ. Correlation coefficients (R) were calculated for each season: DJF (black), MAM (red), JJA (green), and SON (blue).

Based on their findings, here we also try to utilize the ratio of AE values from both shorter and longer wavelength pairs and compare this parameter with the FMF to diagnose the effectiveness as an aerosol size indicator. Using two AE values from different wavelength pairs directly provided from the AERONET data archive, the AE ratio (hereafter, AER) in this study is defined as Eq. (1).

$$AER = \frac{AE\ (500 - 870\ nm)}{AE\ (380 - 500\ nm)} \quad (1)$$

Note that this parameter AER contains similar information (spectral variation of AE) as the parameter α' introduced by Eck et al. (1999) and utilized in the SDA by O'Neill et al. (2001). Similar to Fig. 2, we estimate the correlation between FMF_{500nm} and AER (Fig. 6). Interestingly, AER also has a largely positive correlation with FMF_{500nm} in spite of a little different linear regression shape of the relationship between $AE_{440\text{-}870nm}$ and FMF_{500nm}. While some AER values in summer look deviated from the correlation when the FMF_{500nm} is close to 1.0, R in summer is not as small (R = 0.68 to 0.85). Instead, R values in spring become somewhat smaller (R = 0.61 to 0.85) compared to the springtime correlation between $AE_{440\text{-}870nm}$ and FMF_{500nm}, which is very high (R = 0.85 to 0.95) as shown in Fig. 2. Overall, AER generally captures the FMF variation well in all seasons, indicating that the usage of AER can be an improved approach for the parameterization of relative aerosol size.

Nonetheless, AER also has some complicating features in the Korean summer season. Fig. S13 shows interesting relationships between $AE_{440\text{-}870nm}$ and AER for each season. Generally, $AE_{440\text{-}870nm}$ has moderately positive correlations with AER. In other words, AE from longer wavelengths (hereafter, LW_AE) is larger than AE from shorter wavelengths (hereafter, SW_AE) usually (i.e., AER > 1) when $AE_{440\text{-}870nm}$ is large, but LW_AE smaller than SW_AE usually (i.e., AER < 1) when $AE_{440\text{-}870nm}$ is small. Based on Eck et al. (1999), the case for LW_AE > SW_AE relates to the fine-mode dominant situation, but the LW_AE < SW_AE relates to the coarse-mode dominant case. In addition to $AE_{440\text{-}870nm}$, therefore, AER also describes a spectral aspect of the variation of relative modal aerosol size. However, correlations between $AE_{440\text{-}870nm}$ and AER are quite poor in the Korean summer, which is the main season exhibiting the existence of large fine-mode dominated aerosols.

It seems that very large AER values lead poor correlations with $AE_{440\text{-}870nm}$ in summertime (Fig. S13). Koo et al. (2016) presumed that this large summertime AER probably relates to the existence of brown carbon having the high radiative absorption (300–400 nm) in the ultraviolet wavelength. Brown carbon is one of water-soluble components in the air and its radiative absorption in the short wavelength (~365 nm) can be much amplified if the source is attributed to the anthropogenic emission (Zhang et al., 2011; Chung et al., 2012). It was also found that the dominant source of summertime brown carbon in East Asia is anthropogenic, while biomass burning is more important for the wintertime brown carbon (Laskin et al., 2015). Based on these previous findings, we suppose that the emission and production of anthropogenic brown carbon may be associated with the irregular pattern of AE or AER in Korean summer. Some exceptions occur at the relatively pristine Gangneung_WNU and Gosan_SNU site, showing the moderate linear correlation between $AE_{440\text{-}870nm}$ and FMF_{500nm} (Fig. 2) and also between $AE_{440\text{-}870nm}$ and AER (Fig. S13) in summer, supporting our supposition for the effect of anthropogenic brown carbon. But additional study should be more required in the future to figure out which aerosol component really affects to the irregular pattern of AE in summer.

Anyhow, it is obvious that we have significant uncertainties for the usage of AE as a proxy of aerosol size in Korean summer. Based on Figs. 2 and 6, we can notice some contrasts between the biases in the AE and AER patterns; When the FMF is close to 1.0, some $AE_{440\text{-}870nm}$ values are small, but some AER values are too large. Thus, this suggests that the combination of AE and AER may improve the detection of FMF variation. Therefore, we try to estimate the FMF_{500nm} using a multiple linear regression (MLR) model utilizing both $AE_{440\text{-}870nm}$ and AER data. For each site, we construct the MLR model using 50% data of the $AE_{440\text{-}}$

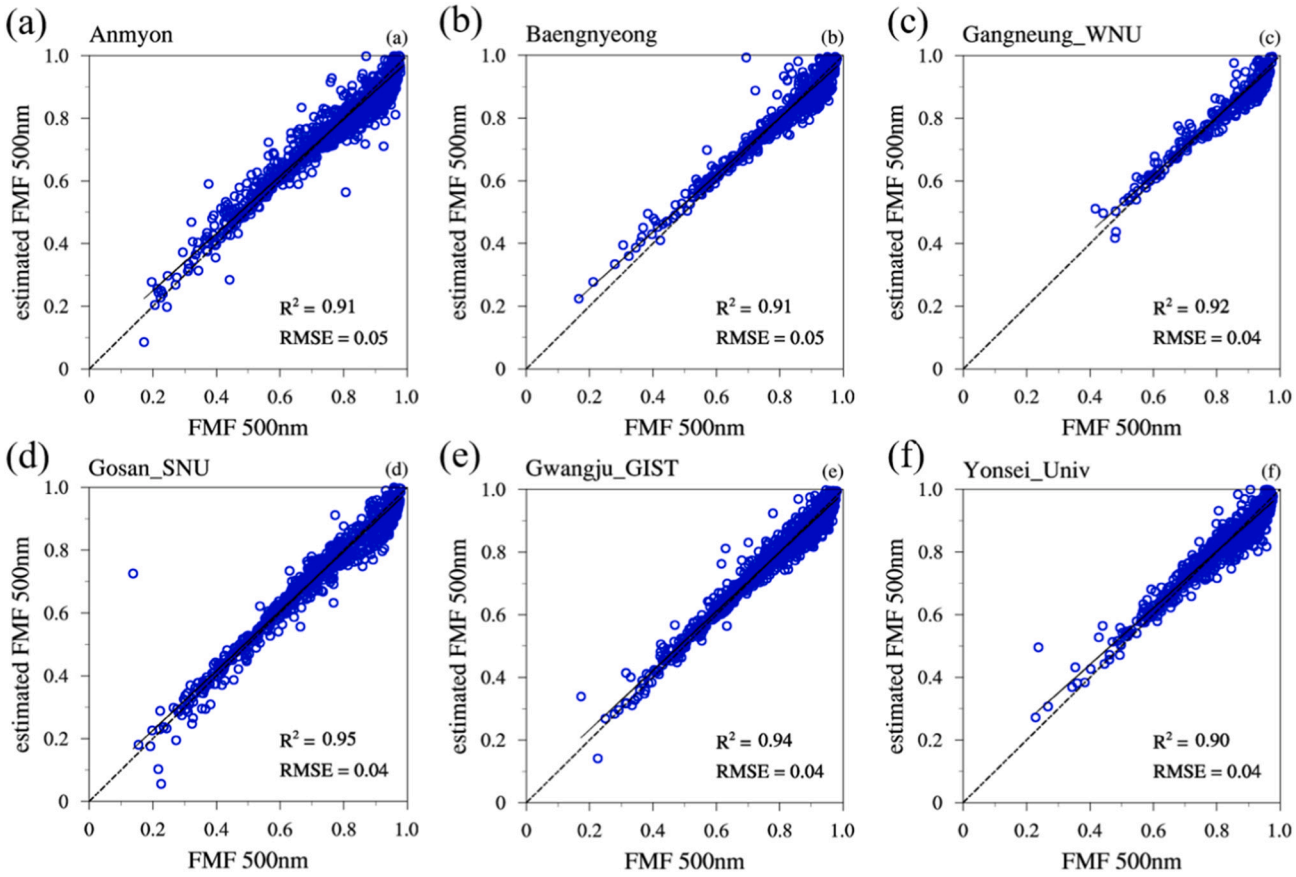

Fig. 7. Linear regression patterns between the FMF_{500nm} from the SDA algorithm (version 3) and estimated FMF_{500nm} based on the MLR model (using $AE_{440\text{-}870nm}$ and AER) at six sites: (a) Anmyon, (b) Baengnyeong, (c) Gangneung_WNU, (d) Gosan_SNU, (e) Gwangju_GIST, and (f) Yonsei_Univ. The coefficient of determination (R^2) and RMSE values are provided for each site.

$_{870nm}$ and AER, and then estimate FMF_{500nm} using the other 50% of the AE and AER values.

Fig. 7 illustrates the relationship between the FMF_{500nm} provided from the AERONET SDA algorithm and our estimated FMF_{500nm}. Surprisingly, all sites show that both FMF values lie on the 1:1 line with R^2 values > 0.9 and root mean square error (RMSE) < 0.05, depicting the remarkable agreement between the original and estimated values. Comparing with results of FMF_{500nm} estimation using the single-variable linear regression model with only $AE_{440\text{-}870nm}$ (Fig. S14) or AER (Fig. S15), the quality of results from the MLR model with both $AE_{440\text{-}870nm}$ and AER shows clearly a large improvement. Results based on version 3 AERONET data are a little better than those with version 2 data, particularly for the part of high FMF (Fig. S16). This seems attributed to better detection of the large fine mode dominance by version 3 data, which is often considered as a cloud contamination and then screened by version 2 data (Eck et al., 2018). Nonetheless, both cases consistently demonstrate the high accuracy of estimated FMF with the MLR model in general.

These findings based on the MLR model indicate the possibility to improve the estimation of regional FMF using only the spectral AOTs, which are required for the calculation of AE and AER (in a wide range in wavelength: e.g., 380 to 870 nm). In other words, aerosol size information can be easily obtained if the high quality of AOTs at multiple channels is guaranteed. Since MLR models at all six sites are quite similar in spite of some regional differences (Table S2), a generalized MLR model applicable to the whole Korean peninsula can be prepared. Then the effort to have a highly accurate AOT enables us to have a better monitoring of both the atmospheric turbidity and the regional aerosol size, revealing the necessity of validation tasks of AOTs (Bright and Gueymard, 2019; Shi et al., 2019). Considering the difficulty to have FMF information directly from the measurement, the usage of AE and AER from the spectral AOT measurement provides a simple and efficient approach.

Lastly, we would discuss about results if the FMF from the inversion algorithm is applied instead of the FMF from the SDA algorithm. We repeat the analysis for the AE-FMF relationship (Fig. S17) and AER-FMF relationship (Fig. S18), and also compare the estimated FMF from our MLR model to the FMF from the inversion algorithm (Fig. S19). It has been known that the inversion algorithm is not available much under the high AOT or partial cloudy situations (Reid et al., 1999), resulted in the lower number of data (Eck et al., 2010). Thus, whole results using the FMF from the inversion algorithm look less significant and some cases cannot be examined well (e.g., wintertime). But the poor AE-FMF correlation and better AER-FMF correlation in Korean summer are similarly found with the usage of FMF values from the inversion algorithm, consistent with our finding related to Figs. 2 and 6. In fact, the degradation of AE-FMF linear relationship in summer occurs more severely; Summertime FMF values from the SDA algorithm still show some sensitivity to the AE change (Fig. 2), but summertime FMF values from the inversion algorithm is mostly larger than 0.8, resulted in insignificant variation (Fig. S17). This feature looks attributed to the difference of 'particle radius cutoff of fine and coarse mode' between two algorithms; some larger fine mode (or smaller coarse mode) particles belongs to the coarse mode in the SDA algorithm, but the fine mode in the inversion algorithm (O'Neill et al., 2003; Eck et al., 2010).

Accordingly, aerosol properties from the SDA algorithm enable to capture the existence of fine mode particle growth better. Nevertheless, estimated FMF values from our MLR models also show large linear correlations with FMF values from the inversion algorithm with R^2 > ~0.8 (Fig. S19). These R^2 values are a little smaller that cases

using the FMF from the SDA algorithm, but still reveal that the MLR model approach using AE and AER is worth to use for the FMF estimation. It is definitely better to use FMF data directly if we have. If not, however, now we can simply derive the FMF using MLR method including AE and AER. It is easy and simple, but efficient and reliable.

4. Summary and conclusion

This study investigated the complicated AE-FMF relationship that occurs in summer over the Korean peninsula. The weak correlation in summer seems associated with the growth of fine mode particle size. The Korean peninsula frequently has very humid and stagnant air conditions along with high air pollutant concentrations in summer, therefore accelerating the hygroscopic growth, cloud processing, and coagulation of fine-mode particles. Since we found that the correlation between FMF and AER is reasonable as the correlation between FMF and $AE_{440\text{-}870nm}$, we came up with a new idea to estimate FMF using both $AE_{440\text{-}870nm}$ and AER based on MLR method. Through the MLR model with utilizing both $AE_{440\text{-}870nm}$ and AER, we estimated FMF with a high degree of accuracy, as compared with the standard AERONET FMF.

Globally, ground-based remote sensing instruments are widely used to observe AOT for the purpose of air quality monitoring: e.g., sunphotometer, skyradiometer, multifilter rotating shadowband radiometer (MFRSR), etc. Although the AERONET system produces the FMF based on both the almucantar inversion algorithm using sunphotometer sky radiance measurements and SDA using spectral AOT only, usually other instruments are only focusing on the measurement or estimation of AOT. Additionally, a number of satellite missions also retrieve spectral AOT measurement successfully, but still have large uncertainties in estimating FMF (Choi et al., 2018). Our MLR model results, however, provide a somewhat simpler way for monitoring of relative aerosol mode contributions (fine versus coarse mode), only requiring the AOT values at multiple channels. It is true that the consistency and high accuracy of spectral AOT values is not easily obtained now. Therefore, much effort should continue to be focused on the high accuracy of AOT retrievals at multiple channels, particularly for the better application of satellite measurement covering the wide range of multiple channels (e.g., Airborne Multiangle SpectroPolarimetric Imager, Xu et al., 2017).

Declaration of Competing Interest

None.

Acknowledgements

This study was supported by the Yonsei University Research Fund of 2019 (2019-22-0011) and grant (NRF-2018R1C1B6008223) from the National Research Foundation of Korea (NRF).

Appendix A. Supplementary data

Supplementary data to this article can be found online at https://doi.org/10.1016/j.atmosres.2020.105217.

References

Alam, K., Khan, R., Sorooshian, A., Blaschke, T., Bibi, S., Bibi, H., 2018. Analysis of aerosol optical properties due to a haze episode in the Himalayan foothills: implications for climate forcing. Aerosol Air Qual. Res. 18, 1331–1350.

Anderson, T.L., Wu, Y., Chu, D.A., Schmid, B., Redemann, J., Dubovik, O., 2005. Testing the MODIS satellite retrieval of aerosol fine-mode fraction. J. Geophys. Res. 110, D18204.

Bright, J.M., Gueymard, C.A., 2019. Climate-specific and global validation of MODIS Aqua and Terra aerosol optical depth at 452 AERONET stations. Sol. Energy 183, 594–605.

Choi, M., Kim, J., Lee, J., Kim, M., Park, Y.-J., Holben, B., Eck, T.F., Li, Z., Song, C.H., 2018. GOCI Yonsei aerosol retrieval version 2 products: an improved algorithm and error analysis with uncertainty estimation from 5-year validation over East Asia. Atmos. Meas. Tech. 11, 385–408.

Chung, C.E., Kim, S.-W., Lee, M., Yoon, S.-C., Lee, S., 2012. Carbonaceous aerosol AAE inferred from in-situ aerosol measurements at the Gosan ABC super site, and the implications for brown carbon aerosol. Atmos. Chem. Phys. 12, 6173–6184.

Dubovik, O., King, M.D., 2000. A flexible inversion algorithm for retrieval of aerosol optical properties from Sun and sky radiance measurements. J. Geophys. Res. 105, 20673–20696.

Dubovik, O., Holben, B.N., Kaufman, Y.J., Yamasoe, M., Smirnov, A., Tanré, D., Slutsker, I., 1998. Single-scattering albedo of smoke retrieved from the sky radiance and solar transmittance measured from ground. J. Geophys. Res. 103, 31903–31923.

Dubovik, O., Holben, B.N., Eck, T.F., Smirnov, A., Kaufman, Y.J., King, M.D., Tanre, D., Slutsker, I., 2002. Variability of absorption and optical properties of key aerosol types observed in worldwide locations. J. Atmos. Sci. 59, 590–608.

Dubovik, O., Sinyuk, A., Lapyonok, T., Holben, B.N., Mishchenko, M., Yang, P., Eck, T.F., Volten, H., Muñoz, O., Veihelmann, B., van der Zande, W.J., Leon, J.-F., Sorokin, M., Slutsker, I., 2006. Application of spheroid models to account for aerosol particle nonsphericity in remote sensing of desert dust. J. Geophys. Res. 111, D11208.

Eck, T.F., Holben, B.N., Reid, J.S., Dubovik, O., Smirnov, A., O'Neill, N.T., Slutsker, I., Kinne, S., 1999. Wavelength dependence of the optical depth of biomass burning, urban, and desert dust aerosols. J. Geophys. Res. 104, 31333–31349.

Eck, T.F., Holben, B.N., Reid, J.S., Sinyuk, A., Dubovik, O., Smirnov, A., Giles, D., O'Neill, N.T., Tsay, S.-C., Ji, Q., Al Mandoos, A., Ramzan Khan, M., Reid, E.A., Schafer, J.S., Sorokine, M., Newcomb, W., Slutsker, I., 2008. Spatial and temporal variability of column integrated aerosol optical properties in the southern Arabian Gulf and United Arab Emirates in summer. J. Geophys. Res. 113, D01204.

Eck, T.F., Holben, B.N., Sinyuk, A., Pinker, R.T., Goloub, P., Chen, H., Chatenet, B., Li, Z., Singh, R.P., Tripathi, S.N., Reid, J.S., Giles, D.M., Dubovik, O., O'Neil, N.T., Smirnov, A., Wang, P., Xia, X., 2010. Climatological aspects of the optical properties of fine/coarse mode aerosol mixtures. J. Geophys. Res. 115, D19205.

Eck, T.F., Holben, B.N., Reid, J.S., Giles, D.M., Rivas, M.A., Singh, R.P., Tripathi, S.N., Bruegge, C.J., Platnick, S., Arnold, G.T., Krotkov, N.A., Carn, S.A., Sinyuk, A., Dubovik, O., Arola, A., Schafer, J.S., Artaxo, P., Smirnov, A., Chen, H., Goloub, P., 2012. Fog- and cloud-induced aerosol modification observed by the Aerosol Robotic Network (AERONET). J. Geophys. Res. 117, D07206.

Eck, T.F., Holben, B.N., Reid, J.S., Arola, A., Ferrare, R.A., Hostetler, C.A., Crumeyrolle, S.N., Berkoff, T.A., Welton, E.J., Lolli, S., Lyapustin, A., Wang, Y., Schafer, J.S., Giles, D.M., Anderson, B.E., Thornhill, K.L., Minnis, P., Pickering, K.E., Loughner, C.P., Smirnov, A., Sinyuk, A., 2014. Observations of rapid aerosol optical depth enhancements in the vicinity of polluted cumulus clouds. Atmos. Chem. Phys. 14, 11633–11656. https://doi.org/10.5194/acp-14-11633-2014.

Eck, T.F., Holben, B.N., Reid, J.S., Xian, P., Giles, D.M., Sinyuk, A., Smirnov, A., Schafer, J.S., Slutsker, I., Kim, J., Koo, J.-H., Choi, M., Kim, K.C., Sano, I., Arola, A., Sayer, A.M., Levy, R.C., Munchak, L.A., O'Neill, N.T., Lyapustin, A., Hsu, N.C., Randles, C.A., Da Silva, A.M., Buchard, V., Govindaraju, R.C., Hyer, E., Crawford, J.H., Wang, P., Xia, X., 2018. Observations of the interaction and transport of fine mode aerosols with cloud and/or fog in Northeast Asia from Aerosol Robotic Network (AERONET) and satellite remote sensing. J. Geophys. Res. Atmos. 123, 5560–5587.

Eck, T.F., Holben, B.N., Kim, J., Beyersdorf, A.J., Choi, M., Lee, S., Koo, J.-H., Giles, D.M., Schafer, J.S., Sinyuk, A., Peterson, D.A., Reid, J.S., Arola, A., Slutsker, I., Smirnov, A., Sorokin, M., Kraft, J., Crawford, J.H., Anderson, B.E., Thornhill, K.L., Diskin, G., Kim, S.-W., Park, S., 2020. Influence of cloud, fog, and high relative humidity during pollution transport events in South Korea: Aerosol properties and PM2.5 variability. Atmos. Environ. 232, 117530.

Giles, D.M., Sinyuk, A., Sorokin, M.G., Schafer, J.S., Smirnov, A., Slutsker, I., Eck, T.F., Holben, B.N., Lewis, J.R., Campbell, J.R., Welton, E.J., Korkin, S.V., Lyapustin, A.I., 2019. Advancements in the Aerosol Robotic Network (AERONET) Version 3 database – automated near-real-time quality control algorithm with improved cloud screening for Sun photometer aerosol optical depth (AOD) measurements. Atmos. Meas. Tech. 12, 169–209.

Gobbi, G.P., Kaufman, Y.J., Koren, I., Eck, T.F., 2007. Classification of aerosol properties derived from AERONET direct sun data. Atmos. Chem. Phys. 7, 453–458.

Holben, B.N., Eck, T.F., Slutsker, I., Tanré, D., Buis, J.P., Setzer, A., Vermote, E., Raegan, J.A., Kaufman, Y.J., Nakajima, T., Lavenu, F., Jankowiak, I., Smirnov, A., 1998. AERONET - a federated instrument network and data archive for aerosol characterization. Remote Sens. Environ. 66, 1–16.

Holben, B.N., Eck, T.F., Slutsker, I., Smirnov, A., Sinyuk, A., Schafer, G., Giles, D., Dubovik, O., 2006. Aeronet's Version 2.0 quality assurance criteria. Proc. SPIE 6408, 64080Q. https://doi.org/10.1117/12.706524.

Kaskaoutis, D.G., Kambezidis, H.D., 2006. Investigation into the wavelength dependence of the aerosol optical depth in the Athens area. Q. J. R. Meteorol. Soc. 132, 2217–2234.

Kim, D.-H., Sohn, B.-J., Nakajima, T., Takamura, T., Takemura, T., Choi, B.-C., Yoon, S.-C., 2004. Aerosol optical properties over East Asia determined from ground-based sky radiation measurements. J. Geophys.Res. 109, D02209. https://doi.org/10.1029/2003JD003387.

Kim, J., Yoon, S.-C., Jefferson, A., Kim, S.-W., 2006. Aerosol hygroscopic properties during Asian dust, pollution, and biomass burning episodes at Gosan, Korea in April 2001. Atmos. Environ. 40, 1550–1560.

Kim, S.-W., Yoon, S.-C., Kim, J., Kim, S.-Y., 2007. Seasonal and monthly variations of columnar aerosol optical properties over East Asia determined from multi-year MODIS, LIDAR, and AERONET sun/sky radiometer measurements. Atmos. Environ. 41, 1634–1651.

Koo, J.-H., Kim, J., Lee, J., Eck, T.F., Lee, Y.G., Park, S.S., Kim, M., Jeong, U., Yoon, J.,

Mok, J., Cho, H.-K., 2016. Wavelength dependence of Ångström exponent and single scattering albedo observed by skyradiometer in Seoul, Korea. Atmos. Res. 181, 12–19.
Laskin, A., Laskin, J., Nizkorodov, S.A., 2015. Chemistry of atmospheric brown carbon. Chem. Rev. 115, 4335–4382. https://doi.org/10.1021/cr5006167.
Lee, J., Kim, J., Song, C.H., Kim, S.B., Chun, Y.S., Sohn, B.J., Holben, B.N., 2010. Characteristics of aerosol types from AERONET sunphotometer measurements. Atmos. Environ. 44, 3110–3117.
Lee, J., Kim, J., Lee, Y.G., 2014. Simultaneous retrieval of aerosol properties and clear-sky direct radiative effect over the global ocean from MODIS. Atmos. Environ. 92, 309–317.
Lee, S., Hong, J., Cho, Y., Choi, M., Kim, J., Park, S.S., Ahn, J.-Y., Kim, S.-K., Moon, K.-J., Eck, T.F., Holben, B.N., Koo, J.-H., 2018. Characteristics of classified aerosol types in the Korean peninsula during the MAPS-Seoul campaign. Aerosol Air Qual. Res. 18, 2195–2206.
Lee, S., Kim, J., Choi, M., Hong, J., Lim, H., Eck, T.F., Holben, B.N., Ahn, J.-Y., Kim, J., Koo, J.-H., 2019. Analysis of long-range transboundary transport (LRTT) effect on Korean aerosol pollution during the KORUS-AQ campaign. Atmos. Environ. 204, 53–67.
Logothetis, S.-A., Salamalikis, V., Kazantzidis, A., 2020. Aerosol classification in Europe, Middle East, North Africa and Arabian peninsula based on AERONET Version 3. Atmos. Res. 239, 104893.
Mok, J., Krotkov, N.A., Torres, O., Jethva, H., Li, Z., Kim, J., Koo, J.-H., Go, S., Irie, H., Labow, G., Eck, T.F., Holben, B.N., Herman, J., Loughman, R.P., Spinei, E., Lee, S.S., Khatri, P., Campanelli, M., 2018. Comparisons of spectral aerosol absorption in Seoul, South Korea. Atmos. Meas. Tech. 11, 2295–2311.
O'Neil, N.T., Royer, A., 1993. Extraction of bimodal aerosol-size distribution raddi from spectral and angular slope (Angstrom) coefficients. Appl. Opt. 32, 1642–1645.
O'Neill, N.T., Dubovik, O., Eck, T.F., 2001. Modified Ångström exponent for the characterization of submicrometer aerosols. Appl. Opt. 40, 2368–2375. https://doi.org/10.1364/AO.40.002368.
O'Neill, N.T., Eck, T.F., Smirnov, A., Holben, B.N., Thulasiraman, S., 2003. Spectral discrimination of coarse and fine mode optical depth. J. Geophys. Res. 108, 4559–4573. https://doi.org/10.1029/2002JD002975.
Randles, C.A., Da Silva, A.M., Buchard, V., Colarco, P.R., Darmenov, A., Govindaraju, R., Smirnov, A., Hoben, B., Ferrare, R., Hair, J., Shinozuka, Y., Flynn, C.J., 2007. The MERRA-2 Aerosol Reanalysis, 1980 Onward. Part I: system description and data assimilation evaluation. J. Clim. 30, 6823–6850.
Reid, J.S., Eck, T.F., Christopher, S.A., Hobbs, P.B., Holben, B.H., 1999. Use of the Ångstrom exponent to estimate the variability of optical and physical properties of aging smoke particles in Brazil. J. Geophys. Res. 104, 27473–27489.
Schuster, G.L., Dubovik, O., Holben, B.N., 2006. Angstrom exponent and bimodal size distributions. J. Geophys. Res. 111, D07207.
Shi, H., Xiao, Z., Zhan, X., Ma, H., Tian, X., 2019. Evaluation of MODIS and two reanalysis aerosol optical depth products over AERONET sites. Atmos. Res. 220, 75–80.
Soni, K., Singh, S., Bano, T., Tanwar, R.S., Nath, S., 2011. Wavelength dependence of the aerosol Angstrom exponent and its implications over Delhi, India. Aerosol Sci. Technol. 45, 1488–1498. https://doi.org/10.1080/02786826.2011.601774.
Valentini, S., Barnaba, F., Bernardoni, V., Calzolai, G., Costabile, F., Di Liberto, L., Forello, A.C., Gobbi, G.P., Gualtieri, M., Lucarelli, F., Nava, S., Petralia, E., Valli, G., Wiedensohler, A., Vecchi, R., 2020. Classifying aerosol partocles through the combination of optical and physical-chemical properties: results from a wintertime campaign in Rome (Italy). Atmos. Res. 235, 104799.
Verma, S., Prakash, D., Ricaud, P., Payra, S., Attié, J.-L., Soni, M., 2015. A new classification of aerosol sources and types as measured over Jaipur, India. Aerosol Air Qual. Res. 15, 985–993. https://doi.org/10.4209/aaqr.2014.07.0143.
Xin, J., Wang, Y., Li, Z., Wang, P., Hao, W.M., Nordgren, B.L., Wang, S., Liu, G., Wang, L., Wen, T., Sun, Y., Hu, B., 2007. Aerosol optical depth (AOD) and Ångström exponent of aerosols observed by the Chinese Sun Hazemeter Network from August 2004 to September 2005. J. Geophys. Res. 112, D05203. https://doi.org/10.1029/2006JD007075.
Xu, F., van Harten, G., Diner, D.J., Kalashnikova, O.V., Seidel, F.C., Bruegge, C.J., Dubovik, O., 2017. Coupled retrieval of aerosol properties and land surface reflection using the airborne multiangle spectropolarimeteric imager. J. Geophys. Res. Atmos. 122, 7004–7026.
Yan, P., Pan, X., Tang, J., Zhou, X., Zhang, R., Zeng, L., 2009. Hygroscopic growth of aerosol scattering coefficient: a comparative analysis between urban and suburban sites at winter in Beijing. Particuology 7, 52–60.
Yoon, J., von Hoyningen-Huene, W., Kokhanovsky, A.A., Burrows, J.P., 2012. Trend analysis of aerosol optical thickness and Ångström exponent derived from the global AERONET spectral observations. Atmos. Meas. Tech. 5, 1271–1299.
Yoon, J., Chang, D.Y., Lelieveld, J., Pozzer, A., Kim, J., Yum, S.S., 2019. Empirical evidence of a positive climate forcing of aerosols at elevated albedo. Atmos. Res. 229, 269–279.
Zhang, X., Lin, Y.-H., Surratt, J.D., Zotter, P., Prévôt, A.S.H., Weber, R.J., 2011. Light-absorbing soluble organic aerosol in Los Angeles and Atlanta: a contrast in secondary organic aerosol. Geophys. Res. Lett. 38, L21810. https://doi.org/10.1029/2011GL049385.
Zheng, F., Hou, W., Sun, X., Li, Z., Hong, J., Ma, Y., Li, L., Li, K., Qiao, Y., 2019. Optimal estimation retrieval of aerosol fine-mode fraction from ground-based sky light measurements. Atmosphere 10, 196. https://doi.org/10.3390/atmos10040196.